Cycloidal Magnetic Gear Combining Axial and Radial Topologies

Godwin Duan, Tanish Gupta, Edward Sutton, Matthew Wang, Matthew C. Gardner, *Member, IEEE*, Salek A. Khan, *Student Member, IEEE*, and Bryton Praslicka, *Student Member, IEEE*

***Abstract*--Axial flux and radial flux cycloidal permanent magnetic gears are characterized by high gear ratios and high torque densities; however, their rotors experience large unbalanced forces, which stress the bearings used in the gear. This paper presents a new cycloidal magnetic gear topology that combines the radial and axial flux topologies. The paper analyzes the forces and torques contributed by the axial and radial magnets in this topology using 3D finite element analysis. It was found that the perpendicular force is necessary to transfer torque to the high-speed shaft and, thus, cannot be cancelled out, but the eccentric component of the magnetic forces can be largely cancelled out, potentially reducing bearing losses and increasing the lifespan of the bearings used in the gear. A proof-of-concept prototype was constructed. Experimental slip torque results matched 3D finite element analysis (FEA) simulations to within 15%, and testing showed that no-load losses were reduced and the slip torque was increased by combining both axial and radial topologies, compared to using an axial configuration alone.**

***Index Terms*-- Axial flux, bearing forces, cycloidal magnetic gear, radial flux, unbalanced magnetic forces.**

I. Introduction

A magnetic gear transfers mechanical power between a low-speed, high-torque shaft and a high-speed, low-torque shaft. However, unlike mechanical gears, magnetic gears transfer power through magnetic fields, rather than physical contact. This provides significant potential advantages over mechanical gears, such as isolation between shafts and inherent overload protection (when too much torque is applied, the gear slips, limiting the maximum torque that is transmitted [1]-[3]). Thus, magnetic gears have attracted significant research interest and have been proposed for various applications, including electric vehicles [4], electric aviation [5], [6], wind turbines [7]-[9], hydrokinetic energy harvesting [10], and actuators for space applications [11], [12].

Most of this research has focused on coaxial magnetic gears [1]-[10], which tend to be limited to relatively low gear ratios, usually less than 12:1 [1]-[10], [13], [14], unless multiple stages are used [9], [14]. On the other hand, cycloidal magnetic gears (CyMGs), which are illustrated in Fig. 1, have demonstrated the ability to achieve high specific torque (torque divided by mass) at high gear ratios [11], [15]-[17], perhaps even comparable to

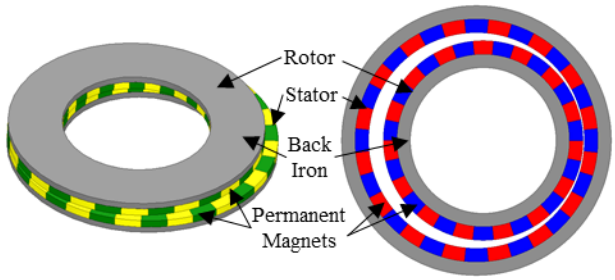

Fig. 1. Example (a) axial flux and (b) radial flux CyMGs.

cycloidal mechanical gears [11]. A CyMG has two rotors with different axes. There are three potential types of motion in a CyMG: (i) the orbit of one rotor's axis about the other rotor's axis, (ii) the rotation of one rotor about its own axis, and (iii) the rotation of the other rotor about its own axis. Usually, one rotor is fixed (this fixed rotor is referred to as the "stator" from this point onwards), and the other rotor both rotates about its own axis and orbits the stator's axis. The stator often has one more pole pair than the rotor:

$$P_{Rot} = P_{Sta} - 1, \tag{1}$$

where P_{Rot} is the number of rotor pole pairs and P_{Sta} is the number of stator pole pairs [11], [15]-[19], [21], [22]. Then, the gear ratio (G) relates the orbital speed (ω_{Orb}) of the rotor's axis about the axis of the stator to the rotor's rotational speed (ω_{Rot}) about its own axis, according to

$$G = \frac{\omega_{Orb}}{\omega_{Rot}} = -P_{Rot}. \tag{2}$$

This motion is illustrated in Fig. 2 for an example radial flux CyMG [15]. The relationships in (1) and (2) allow CyMGs to achieve large gear ratios without having to have two very different pole counts on the stator and the rotor, providing a significant performance advantage over coaxial magnetic gears at high gear ratios [15].

Both axial flux and radial flux CyMGs have been proposed and prototyped [11], [15]-[19]. For the axial flux CyMG, which is illustrated in Fig. 1(a), the offset between the axes produces a region where there is large overlap between the rotor and stator permanent magnets (PMs), which is where most of the magnetic interaction occurs, and an opposite region where there is much less overlap between the rotor and stator PMs, where much less magnetic interaction occurs [18]. For the radial flux

G. Duan, T. Gupta, E. Sutton, and M. Wang were with the CAST-STEM Bridge Summer Camp, Richardson, TX 75080 USA.

M. C. Gardner and S. A. Khan are with the University of Texas at Dallas, Richardson, TX 75080 USA (e-mail: matthew.gardner@utdallas.edu and salek@utdallas.edu).

B. Praslicka is with Texas A&M University and FluxWorks LLC, College Station, TX 77843, USA (e-mail: bryton.praslicka@tamu.edu).

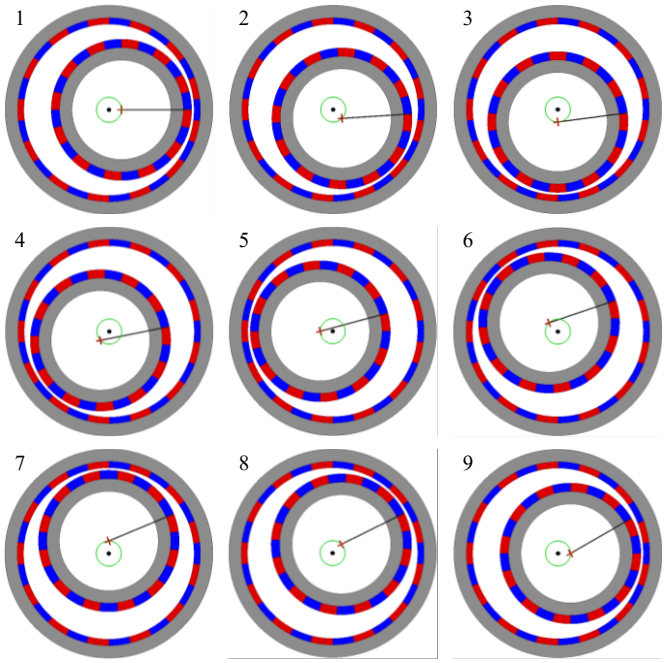

Fig. 2. Example cycloidal magnetic gear operation motion sequence. The inner rotor's axis (red '+') orbits the outer rotor's axis (black dot) along the green path while the inner rotor rotates about its own axis [15].

CyMG, which is illustrated in Fig. 1(b), there is a region with a small airgap, which is where most of the magnetic interaction occurs, and a region with a large airgap, where much less magnetic interaction occurs [16].

However, CyMGs present significant mechanical challenges [11], [18], [19]. First, the center of mass moves, which can cause undesirable vibrations, unless the rotor is divided into multiple sections [11], [17] or a counterweight is employed [18], [19]. Second, the orbital motion of the rotor about the axis of the stator must be decoupled from the rotor's rotation about its own axis. This often involves using internal roller pins which experience large forces and can create significant frictional losses [11], but alternative approaches involving large quantities of PMs to achieve this decoupling without pins have been proposed [18], [20]. Third, the PMs create large unbalanced forces, which must be supported by the central bearing between the rotor and the high-speed shaft [11]. These forces can reduce the life of the bearing and the gear's efficiency [11]. One dual-rotor arrangement involving axial flux CyMGs has been proposed to largely cancel out the unbalanced magnetic forces that must pass through the bearing [21]. However, this arrangement has significant disadvantages, including reduced torque density (because both stages must be sized for approximately the same torque as the low-speed shaft torque) and either a reduced gear ratio or circulating power. The gear ratio can be increased in a manner similar to the compound differential coaxial magnetic gear in [14], resulting in the same problem with circulating power, which can lead to low efficiencies. Nonetheless, [21] did demonstrate that the magnetic forces in the direction of the axis offset can be balanced in a single-stage axial flux CyMG through careful selection of the design parameters.

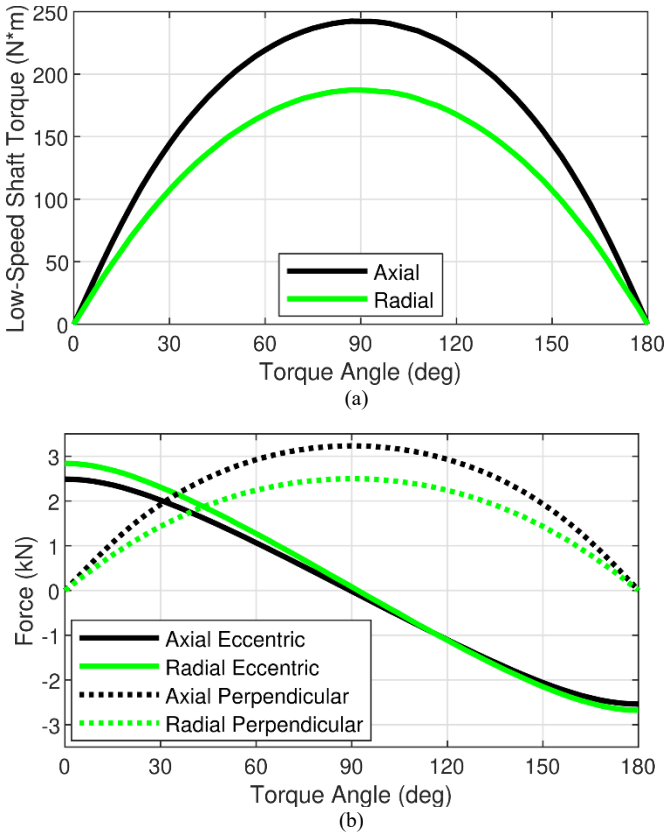

Fig. 3. (a) Torques and (b) forces for the axial flux and radial flux CyMGs depicted in Fig. 1.

Fig. 3 illustrates the variation of the magnetic forces and torque on the rotor as the torque angle changes for the axial flux CyMG illustrated in Fig. 1(a) and the radial flux CyMG illustrated in Fig. 1(b). The forces in the direction of the axis offset are called the eccentric forces, and the forces perpendicular to the axis offset are called the perpendicular forces. (If the rotor's axis is offset in the +x direction, the eccentric force is in the +x direction, the perpendicular force is in the +y direction, and positive torque is defined as counterclockwise when viewed from above.) Both the torques and perpendicular forces vary sinusoidally with the torque angle. The eccentric forces vary cosinusoidally with the torque angle. However, the eccentric force for the radial flux gear has a slight offset, such that there is a small but nonzero eccentric force at a 90 degree torque angle, as in [22]. This paper proposes a CyMG that combines the radial flux and axial flux CyMG topologies. The goal of proposing this topology is to reduce the net magnetic forces acting on the rotor. This topology and the investigation of the magnetic forces are described in the remaining sections of this paper.

II. Hypothesis

Fig. 4 illustrates the proposed topology combining axial flux and radial flux CyMGs. Note that each PM arrangement on the rotor has the same number of pole pairs (P_{Rot}), and each PM arrangement on the stator has the same number of pole pairs (P_{Sta}). In Fig. 4(b), the radial flux (red and blue magnets) portion of the stator has a larger diameter than the radial flux portion of the rotor. However, the axial flux (yellow and green magnets)

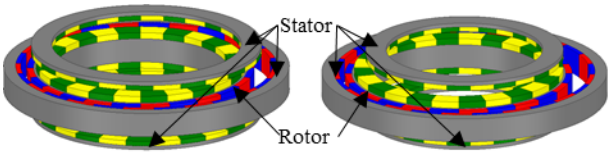

(a) (b)

Fig. 4. Example CyMGs combining radial flux and axial flux topologies, with (a) both the radial and axial stator magnets having larger radii than the radial and axial rotor magnets or (b) with the radial stator magnets having larger radii than the radial rotor magnets but the axial stator magnets having smaller radii than the axial rotor magnets.

portion of the stator has a smaller diameter than the axial flux portion of the rotor. Thus, the small airgap region of the radial flux portion of the gear is on the opposite side of the shaft from the large overlap region of the axial flux portion. We hypothesized that this would allow the perpendicular and eccentric forces of the radial flux and axial flux portions of the gear to largely cancel out, while their torques would add up. This hypothesis is based on the observation that the primary torque producing regions of the radial flux (small airgap region) and axial flux (large overlap region) portions of the gear are opposite each other, so we assumed the forces producing positive torque in the radial flux portion would oppose the forces producing positive torque in the axial flux portion.

III. Design Study

It has already been demonstrated that the magnitude and sign of the eccentric forces in an axial flux CyMG can be manipulated [21]. To investigate whether it is possible to change the sign of the perpendicular forces in an axial flux CyMG, a 3D parametric magnetostatic finite element analysis (FEA) design sweep was performed using ANSYS Maxwell. (While an analytical model for radial flux CyMGs has been proposed, it has demonstrated relatively poor accuracy, due to its inability to account for 3D effects [17].) For this study, the pole pair counts were related by (1), but the stator was given a smaller diameter than the rotor, as in the axial portions of Fig. 4(b). The design parameters evaluated for the sweep are shown in Table I. The rotor's outer ($R_{Rot,out}$) and inner ($R_{Rot,in}$) radii and the stator's outer ($R_{Sta,out}$) and inner ($R_{Sta,in}$) radii are given by

$$R_{Rot,out} = R_{Nom} + O_{Rout}, \quad (3)$$

$$R_{Rot,in} = k_R R_{Nom} + O_{Rin}, \quad (4)$$

$$R_{Sta,out} = R_{Nom} - O_{Axis}, \quad (5)$$

$$R_{Sta,in} = k_R R_{Nom} - O_{Axis}. \quad (6)$$

The rotor back irons were assumed to be tape-wound 29-gauge M15 electrical steel, and the PMs were assumed to be N50H at room temperature. Each design was evaluated at both the zero torque and peak torque angles.

Fig. 5 shows the relationship between the torque at the peak torque angle, the eccentric force at the zero-torque angle, and the perpendicular force at the peak torque angle. Fig. 5(a) shows that the sign of the eccentric forces can be changed and their magnitudes varied over a wide range, which agrees with the results in [21]. However, the sign of the perpendicular force only changes when the torque at the peak torque angle changes sign. Thus, to cancel out the perpendicular forces, the torque generated by the axial portions would have to oppose the torque

TABLE I
Axial Flux Design Study Parameters

Symbol	Description	Values
P_{Rot}	Rotor pole pairs	20, 30 ,40
R_{Nom}	Nominal outer radius	100 mm
k_R	Nominal radii ratio	0.5, 0.625, 0.75
O_{Rin}	Rotor inner radius offset	-9, -6, -3, … 9 mm
O_{Rout}	Rotor outer radius offset	-9, -6, -3, … 9 mm
T_{BI}	Back iron axial thicknesses	5 mm
T_{PM}	Magnet axial thicknesses	6 mm
T_{AG}	Airgap	1 mm
O_{Axis}	Axis offset	3, 6, 9, 12 mm

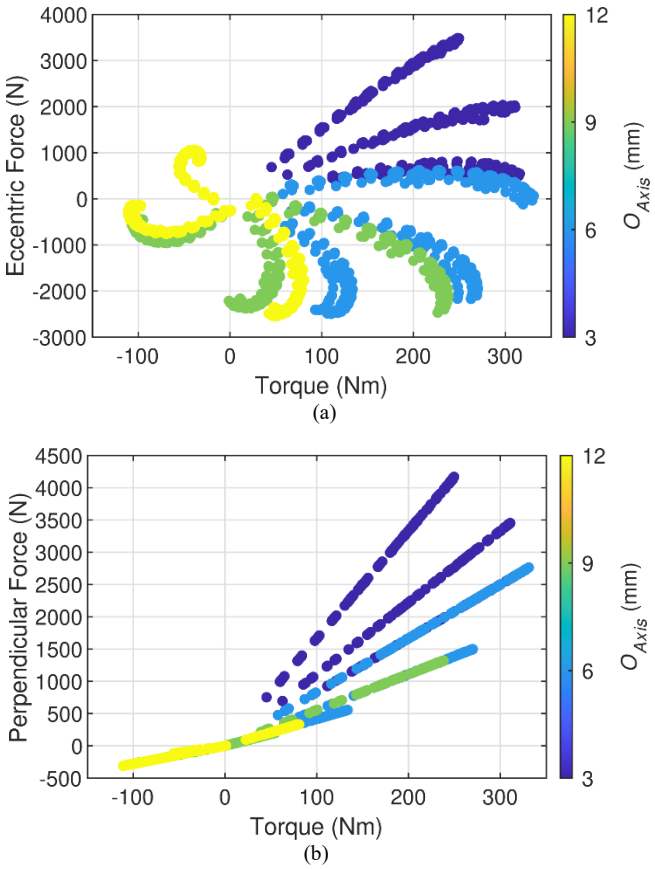

(a)

(b)

Fig. 5. Low-speed shaft torque at the peak torque angle and (a) eccentric forces at the no-load angle or (b) perpendicular forces at the peak torque angle for different axis offsets from the axial flux design study results.

generated by the radial portion. Therefore, the hypothesis was partially discredited, the perpendicular forces could not be cancelled without the radial and axial portions generating opposing torques. The assumption that the forces generated in the large overlap region would be dominant was flawed; magnets throughout each design contributed significant forces, as in [21].

Further inspection of the data depicted in Fig. 5(b) reveals a pattern. The perpendicular forces are necessary to transfer the high-speed shaft torque from the rotor to the high-speed shaft. Thus, the perpendicular force of a design is related to its low-speed shaft torque according to

$$F_{Perp} = \frac{\tau_{LS}}{P_{Rot} O_{Axis}}, \quad (7)$$

where F_{Perp} is the perpendicular force and τ_{LS} is the low-speed

shaft torque. This relationship holds for all the designs in the study, within the bounds of numerical error, and is unaffected by other geometric parameters. Additionally, due to the nature of this relationship, (7) should hold for both axial flux and radial flux designs [21]. Thus, the perpendicular force can be reduced by increasing the magnitude of the gear ratio (related to P_{Rot} by (2)), which reduces the high-speed shaft torque for a given low-speed shaft torque, or by increasing the axis offset, which provides a larger torque arm for applying torque to the high-speed shaft; however, increasing the gear ratio generally reduces the optimal axis offset [11], [15]. This relationship indicates that it would be impossible to use the axial portion of the gear to cancel out the perpendicular forces on the central bearing without cancelling out the torques. Thus, there was no advantage to making the stator radius smaller than the rotor radius for the axial flux portion of the gear.

IV. Plan B

Therefore, we decided to make the radii of the axial portions of the stator larger than the radius of the axial portion of the rotor, as illustrated in Fig. 4(a). In this configuration, the eccentric forces from the radial magnets can be cancelled by negative eccentric forces from the axial magnets. The net magnetic eccentric force from the magnets remains low under no load and stays at a constant low value up to the peak torque angle.

Force applied to a bearing during operation increases its friction, consequently increasing the losses of the gearbox. Using both axial and radial magnets, we are able to reduce the eccentric force on the rotor, reducing the forces on the bearings between the rotor and the high-speed shaft; therefore, we would expect the no-load losses of this type of gear to be lower than if it only had a radial or axial configuration alone.

V. Proof-of-Concept Prototype

The prototype was built over the course of a six-week summer camp, restricting us to using only off-the-shelf or additively manufactured parts. We evaluated a range of geometric parameters based on available components to identify a design with minimal net eccentric forces on the rotor. Table II shows the design parameter values for the 20:1 cycloidal magnetic gear prototype. Figs. 6(a), (b), and (c) show

TABLE II
Prototype Gear Design Parameters

Description	Values
Rotor pole pairs	20
Stator pole pairs	21
Magnet material	Neodymium N50
Axial magnet dimensions	12.7 mm x 6.4 mm x 3.2 mm
Radial magnet dimensions	19.1mm x 9.5mm x 3.2 mm
Rotor back iron dimensions	126.8 mm OD, 101.6 mm ID, 22.9 mm length
Radial stator back iron dimensions	177.5 mm OD, 164.8 mm ID, 22.9 mm length
Axial back iron dimensions	139.6 mm OD, 114.2 mm ID, 3mm thick
Minimum radial airgap	6.1 mm
Axial airgap	5 mm
Axis offset	6.4 mm

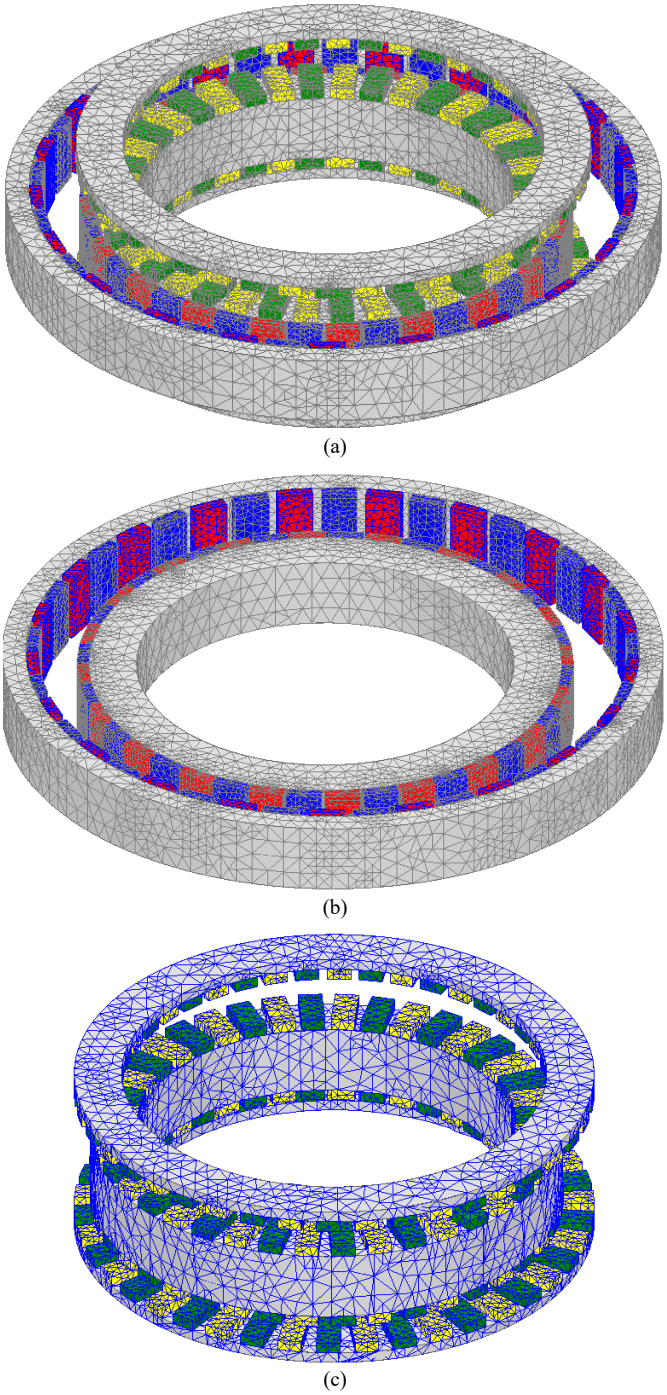

Fig. 6. The mesh generated by ANSYS Maxwell's magnetostatic adaptive meshing for (a) the configuration with both axial and radial flux, (b) the radial flux only configuration, and (c) the axial flux only configuration.

the mesh for the simulation of the whole prototype, the radial portion only, and the axial portion only, and Table III provides the number of tetrahedra used in the mesh and the simulation time. Figs. 7(a), (b), and (c) show the simulated torques, eccentric forces, and perpendicular forces on the rotor as a function of the low-speed shaft angle for one half of an electromagnetic cycle (1 pole span).

Fig. 8 shows cutaway and exploded views of the prototype. The enclosure for the prototype gear consists of two halves, additively manufactured with PETG, allowing for ease of assembly. Low-carbon, magnetic steel pipe was used as a back

TABLE III
PROTOTYPE SIMULATION COMPARISON

	A: All Magnets	B: Radial Only	C: Axial Only
Number of Tetrahedra	821887	630665	264135
Simulation Time	2423 s	1587 s	559 s

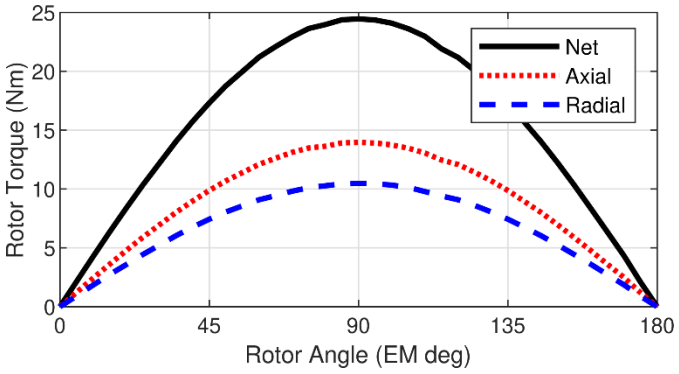

(a)

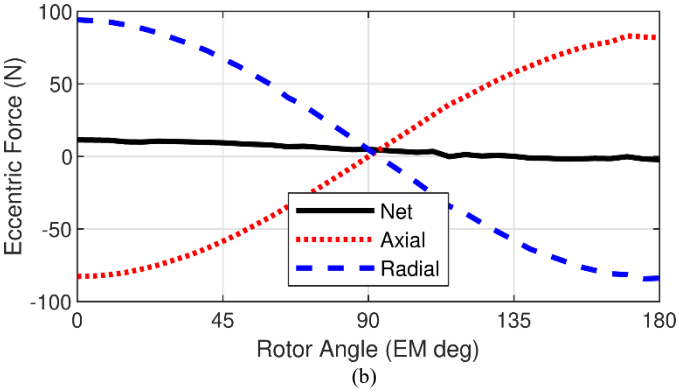

(b)

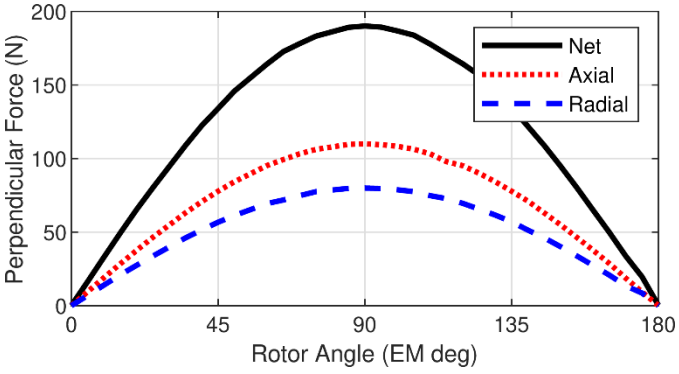

(c)

Fig. 7. The simulated (a) torques, (b) eccentric forces, and (c) perpendicular forces for the prototype.

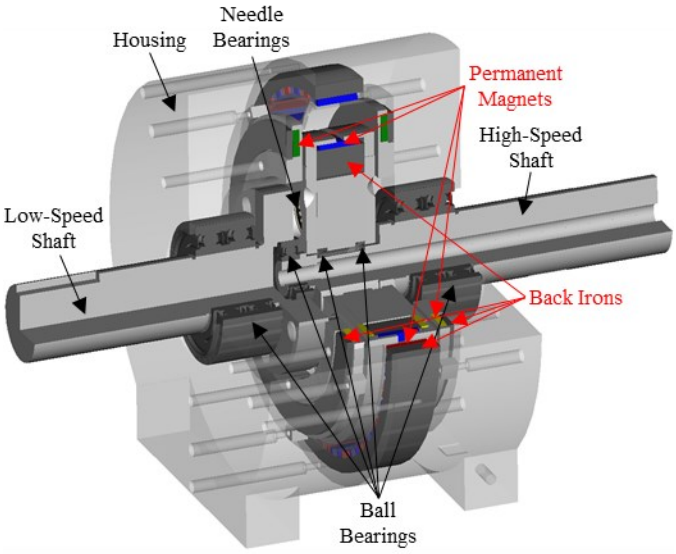

(a)

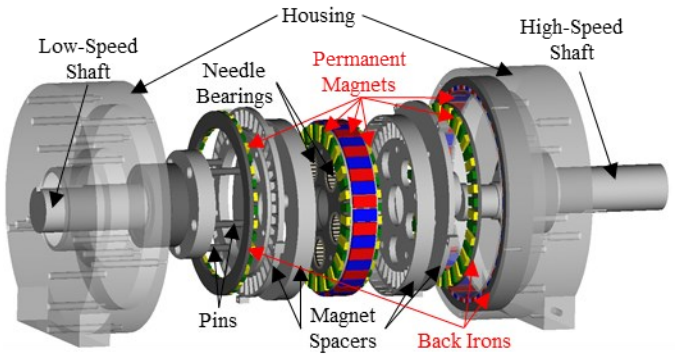

(b)

Fig. 8. (a) Cutaway and (b) exploded views of the prototype design. Structural components are annotated in black and magnetically active components in red.

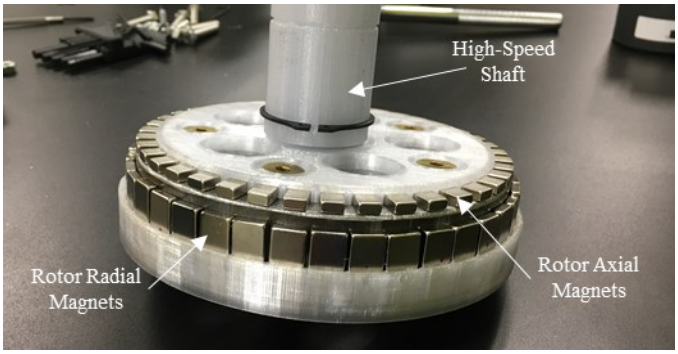

Fig. 9. The rotor assembly, pictured with one spacer removed to show magnet layout.

iron for the radial stator, and as the body of the rotor. Two flat, circular cutouts of magnetic steel sheet metal were used as back irons for the axial stator magnets. Stator magnets were aligned and held in place using additively manufactured spacers, which were then mounted onto the inside of the enclosure with screws, ensuring that they were all aligned with respect to each other. Rotor magnets were aligned in a similar way, with their spacers attached to the body of the rotor, shown in Fig. 9.

The high-speed and low-speed shafts are held in place by two ball bearings each, mounted inside the face of the enclosure. Additionally, in order to prevent the shafts from being cantilevered, a nested bearing was used, with the outer race on the low-speed shaft, and the inner race on the high-speed shaft. The shafts and rotor are pressed into place with a wave spring when securing the two halves of the enclosure together. A counterweight was placed on the high-speed shaft opposite to the offset of the rotor, to counteract torque ripple caused by gravity acting on the inherently unbalanced eccentric rotor. Fig. 10 shows the inside of the prototype.

The prototype was tested for slip torque and no-load losses in three configurations: Configuration A, with all axial and radial magnets in place; Configuration B, with all magnets

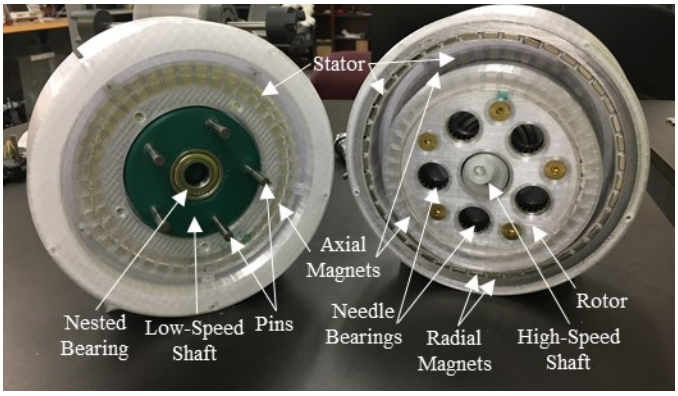

Fig. 10. The two halves of the enclosure. The green low-speed shaft contains the pins that couple to the rotor's rotation about its own axis. The radial stator is embedded into the high-speed shaft side of the enclosure (right half), where the rotor is installed.

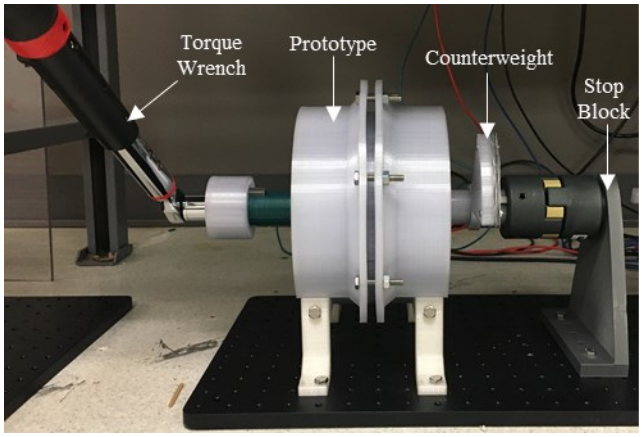

(a)

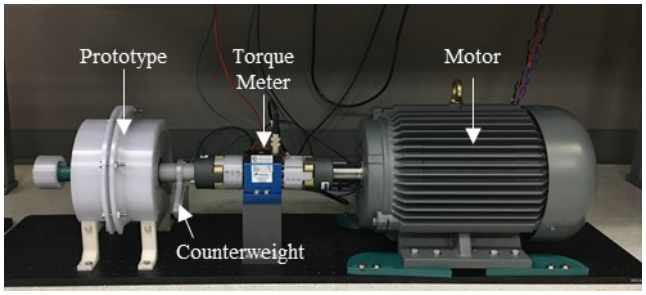

(b)

Fig. 11. The prototype on the test bed for (a) slip torque testing and (b) no-load loss testing.

except the axial stator magnets in place; and Configuration C, with all magnets except the radial rotor magnets in place. In Configuration A, all the magnets produce torques and forces. However, in Configuration B, the radial magnets produce the vast majority of the torques and forces, and, in Configuration C, the axial magnets produce the vast majority of the torques and forces. Figs. 11(a) and (b) show the prototype on the test bed.

Table IV compares the experimental slip torque measurements with the 3D FEA predictions. We fixed the high-speed shaft and turned the low-speed shaft with a torque wrench to measure the slip torque, as shown in Fig. 11(a). Even after repeatedly overloading the gear, causing it to slip, the slip torque remained consistent, indicating that no significant

TABLE IV
SIMULATED AND MEASURED SLIP TORQUES

Configuration	3D FEA Slip Torque	Measured Slip Torque
A: All Magnets	24.5 Nm	20.9 Nm
B: Without Axial Stator Magnets	10.5 Nm	8.2 Nm
C: Without Radial Rotor Magnets	14.3 Nm	12.8 Nm

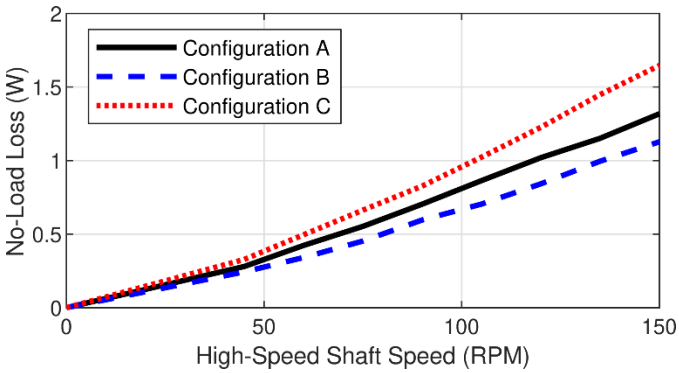

Fig. 12 The no load losses of the prototype of the 3 configurations, tested across a range of high-speed shaft speeds.

demagnetization occurred. Fig. 12 shows the measured no load losses for each of the three configurations. To measure no-load losses, we connected the high-speed shaft to an induction motor through a torque meter and allowed the low-speed shaft to spin freely, as shown in Fig. 11(b). The no-load loss was calculated as the product of the torque on the high-speed shaft and its speed when the low-speed shaft was allowed to spin freely in steady-state.

The results show that Configuration A, which had all the magnets in place, had a higher slip torque than Configurations B and C and lower losses than Configuration C. This supports our expectation that the reduced eccentric force on the bearing would result in lower no-load losses. However, Configuration B, which had axial stator magnets removed, had lower losses than both of these configurations. Thus, the experiment did not fully match our expectation that the gear with both axial and radial magnets would have lower losses than a gear with either axial or radial magnets individually. This may be explained by the two axial airgaps being unequal, which would create an unbalanced axial force on the bearings, increasing frictional losses. Due to fabrication tolerances, especially with additively manufactured components, it is possible there was a significant imbalance in the axial airgaps. The unequal airgaps could also explain the discrepancies between the simulated and measured slip torques. Additionally, uneven spacing between radial rotor magnets (Fig. 9) may have reduced the measured torque in Configurations A and B.

The prototype possessed several non-optimal structural design features. First, strictly using off-the-shelf parts meant a mechanically and magnetically optimal design could not be achieved; for example, the 6.4 mm axis offset was determined by the size of available pins and bearings. Second, five needle bearings without an inner race, like the one shown in Fig. 13, were used in the rotor body to couple the rotor's orbital motion to the low-speed shaft. However, since individual needles of the bearing were exposed and similar in diameter to the pins, the pins bumpily rolled around them during operation, undoubtedly

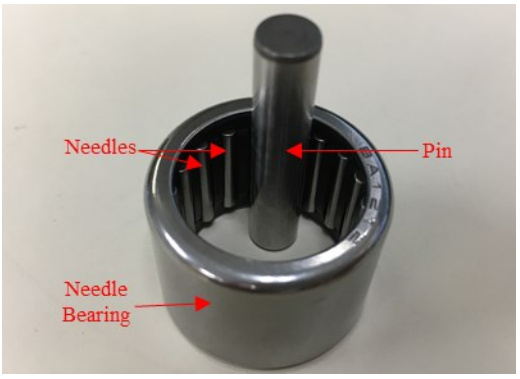

Fig. 13. The needle bearing and pin used to couple rotational motion to the low-speed shaft.

increasing the losses and torque ripple of the gear. Third, the counterweight may have under- or over-compensated for the eccentric rotor, leading to torque ripple and variations in measured slip torque. Fourth, large effective magnetic airgaps, which reduced the torque, were used to increase the probability of having a working prototype within the six-week constraint. Finally, the materials used for the additively manufactured components had lower stiffness than materials conventionally used with conventional machining.

Table V compares the performance of the three prototype configurations. For Configuration B, it was assumed that all axial flux magnets and the stator axial flux back irons were removed, as shown in Fig. 6(b). For Configuration C, it was assumed that all radial flux magnets and the stator radial flux back iron were removed, as shown in Fig. 6(c). This is slightly different than how the experiments were conducted because of the way the prototype was assembled. However, simulations indicated that there would be a negligible difference in torque between removing the axial stator magnets only and removing the axial flux magnets on both the rotor and stator. Similarly, simulations indicated that there would be a negligible difference in torque between removing the radial stator magnets only and removing the radial flux magnets on both the rotor and stator.

While Table V does not compare optimized representatives of each topology, a few conclusions can be drawn. The torque density of the combined axial flux and radial flux topology (Configuration A) benefits from using both the axial and radial air gap surfaces. (The torque density is still relatively low due to the conservatively large magnetic airgaps.) Configuration A cannot have the highest torque per magnet mass of the three configurations because its torque is approximately the sum of the torques of the other two configurations, and its magnet mass is also the sum of the magnet masses of the other two configurations. Configuration A achieves a higher ratio of slip torque to rotor inertia than the other topologies because, while Configuration A has a higher torque than the other configurations, all three configurations share many of the same rotor components. This may be advantageous in applications requiring quick dynamic performance. While a dynamic analysis of the different configurations is beyond the scope of this paper, [23]-[26] have provided analyses of the dynamic performance of magnetic gears.

TABLE V
PROOF-OF-CONCEPT PROTOTYPE CONFIGURATION COMPARISON

	A: All Magnets	B: Radial Only	C: Axial Only
Slip Torque	20.9 Nm	8.2 Nm	12.8 Nm
Active Torque Density	17.6 kNm/m^3	16.9 kNm/m^3	17.5 kNm/m^3
Number of Magnets	246	82	164
Magnet Mass	0.67 kg	0.35 kg	0.31 kg
Torque/Magnet Mass	31.2 Nm/kg	23.2 Nm/kg	40.6 Nm/kg
Rotor Inertia about Own Axis	36.3 kg·cm^2	31.3 kg·cm^2	29.0 kg·cm^2

VI. CONCLUSION

This paper proposes and analyzes a new cycloidal magnetic gear topology combining axial and radial flux CyMG's, resulting in several conclusions:

- A cycloidal magnetic gear with a radial stator larger than the rotor and an axial stator smaller than the rotor was initially proposed. Fig. 5 demonstrates that in this configuration, it is possible to cancel out the net eccentric magnetic forces but not the net perpendicular magnetic forces without cancelling the torques.
- However, the net eccentric forces can still be cancelled if both the radial stator and axial stator radii are larger than the rotor radius.
- The perpendicular magnetic forces are what transfers torque to the high-speed shaft and can be related to the low-speed shaft torque based on the gear ratio and the axis offset according to (7).
- A proof-of-concept prototype demonstrated smaller no-load losses and higher slip torque with both axial and radial magnets present than with only axial magnets present.

The prototype in this paper presents the first proof-of-concept demonstration of a combined axial flux and radial flux cycloidal magnetic gear in the literature. However, higher slip torques, torque densities, and lower losses could have been achieved with the use of custom machined parts. Further study is needed to determine how the efficiency and reliability of more optimal axial-radial cycloidal magnetic gears compare to conventional magnetic and mechanical gears.

VII. ACKNOWLEDGMENT

The authors would like to thank the organizers of the 2021 CAST STEM Bridge Camp for the opportunity to have high school students conduct research at the University of Texas at Dallas.

VIII. REFERENCES

[1] G. Cooke, R.-S. Dragan, R. Barrett, D. J. Powell, S. Graham, and K. Atallah, "Magnetically Geared Propulsion Motor for Subsea Remote Operated Vehicle," *IEEE Trans. Magn.*, vol. 58, no. 2, pp. 1-5, Feb. 2022.

[2] S. S. Nielsen, R. K. Holm, and P. O. Rasmussen, "Conveyor System With a Highly Integrated Permanent Magnet Gear and Motor," *IEEE Trans. Ind. Appl.*, vol. 56, no. 3, pp. 2550-2559, May-Jun. 2020.

[3] M. Bouheraoua, J. Wang, and K. Atallah, "Slip Recovery and Prevention in Pseudo Direct Drive Permanent-Magnet Machines," *IEEE Trans. Ind. Appl.*, vol. 51, no. 3, pp. 2291-2299, May-Jun, 2015.

[4] T. V. Frandsen et al., "Motor integrated permanent magnet gear in a battery electrical vehicle," *IEEE Trans. Ind. Appl.*, vol. 51, no. 2, pp. 1516-1525, Mar.-Apr. 2015.

[5] J. J. Scheidler, V. M. Asnani and T. F. Tallerico, "NASA's magnetic gearing research for electrified aircraft propulsion," in *Proc. AIAA/IEEE Elect. Aircraft Technol. Symp.*, 2018, pp. 1-12.
[6] T. F. Tallerico, Z. A. Cameron and J. J. Scheidler, "Design of a magnetic gear for NASA's Vertical Lift Quadrotor Concept Vehicle," in *Proc. AIAA/IEEE Elect. Aircraft Technol. Symp.*, 2019, pp. 1-21.
[7] N. W. Frank and H. A. Toliyat, "Gearing ratios of a magnetic gear for wind turbines," in *Proc. IEEE Int. Elect. Mach. Drives Conf.*, 2009, pp. 1224–1230.
[8] A. B. Kjaer, S. Korsgaard, S. S. Nielsen, L. Demsa and P. O. Rasmussen, "Design, fabrication, test, and benchmark of a magnetically geared permanent magnet generator for wind power generation," *IEEE Trans. Energy Conv.*, vol. 35, no. 1, pp. 24-32, Mar. 2020.
[9] K. Li, S. Modaresahmadi, W. B. Williams, J. D. Wright, D. Som, and J. Z. Bird, "Designing and experimentally testing a magnetic gearbox for a wind turbine demonstrator," *IEEE Trans. Ind. Appl.*, vol. 55, no. 4, pp. 3522-3533, Jul.-Aug. 2019.
[10] M. Johnson, M. C. Gardner, H. A. Toliyat, S. Englebretson, W. Ouyang, and C. Tschida, "Design, construction, and analysis of a large scale inner stator radial flux magnetically geared generator for wave energy conversion," *IEEE Trans. Ind. Appl.*, vol. 54, no. 4, pp. 3305–3314, Jul.-Aug. 2018.
[11] B. Praslicka *et al.*, "Practical analysis and design of a 50:1 cycloidal magnetic gear with balanced off-axis moments and a high specific torque for lunar robots," in *Proc. IEEE Int. Elect. Mach. and Drives Conf.*, 2021, pp. 1-8.
[12] G. Puchhammer, "Magnetic gearing versus conventional gearing in actuators for aerospace applications," in *Proc. Aero. Mech. Symp.*, 2014, pp. 175-181.
[13] B. Praslicka, M. C. Gardner, M. Johnson, and H. A. Toliyat, "Review and analysis of coaxial magnetic gear pole pair count selection effects," *IEEE Trans. Emerg. Sel. Topics Power Electron.*, vol. 10, no. 2, pp. 1813-1822, Apr. 2022.
[14] M. C. Gardner, M. Johnson, and H. A. Toliyat, "Analysis of high gear ratio capabilities for single-stage, series multistage, and compound differential coaxial magnetic gears," *IEEE Trans. Energy Convers.*, vol. 34, no. 2, pp. 665-672, Jun. 2019.
[15] M. C. Gardner, M. Johnson, and H. A. Toliyat, "Comparison of surface permanent magnet coaxial and cycloidal radial flux magnetic gears," in *Proc. IEEE Energy Convers. Congr. and Expo.*, 2018, pp. 5005-5012.
[16] J. Rens, K. Atallah, S. D. Calverley, and D. Howe, "A novel magnetic harmonic gear," *IEEE Trans. Ind. Appl.*, vol. 46, no. 1, pp. 206-212, Jan.-Feb. 2010.
[17] F. T. Jørgensen, T. O. Andersen, and P. O. Rasmussen, "The cycloid permanent magnetic gear," *IEEE Trans. Ind. Appl.*, vol. 44, no. 6, pp. 1659-1665, Nov.-Dec. 2008.
[18] K. Davey, L. McDonald, and T. Hutson, "Axial flux cycloidal magnetic gears," *IEEE Trans. Magn.*, vol. 50, no. 4, pp. 1-7, Apr. 2014.
[19] K. Davey, T. Hutson, L. McDonald and G. Hutson, "The design and construction of cycloidal magnetic gears," in *Proc. IEEE Int. Elect. Mach. and Drives Conf.*, 2017, pp. 1-6.
[20] B. Juraj, B. Ronals, M. Rudolf, and P. Silvester, "Two-way magnetic cycloid gearbox," Slovakia Patent, SK8188 Y1, Aug. 2, 2018.
[21] H. Huang, J. Z. Bird, A. L. Vera, and R. Qu, "An axial cycloidal magnetic gear that minimizes the unbalanced radial force," *IEEE Trans. Magn.*, vol. 56, no. 7, pp. 1-10, Jul. 2020.
[22] M. Johnson, S. Hasanpour, M. C. Gardner, and H. A. Toliyat, "Analysis and benchmarking of radial flux cycloidal magnetic gears with reduced permanent magnet piece count using consequent poles", in *Proc. IEEE Energy Convers. Congr. Expo*, 2021, pp. 1-8.
[23] S. Pakdelian, M. Moosavi, H. A. Hussain, and H. A. Toliyat, "Control of an Electric Machine Integrated With the Trans-Rotary Magnetic Gear in a Motor Drive Train," *IEEE Trans. Ind. Appl.*, vol. 53, no. 1, pp. 106-114, Jan.-Feb. 2017.
[24] M. C. Gardner and H. A. Toliyat, "Nonlinear Analysis of Magnetic Gear Dynamics Using Superposition and Conservation of Energy," in *Proc. IEEE Int. Elect. Mach. and Drives Conf.*, 2019, pp 210-217.
[25] T. V. Frandsen, N. I. Berg, R. K. Holm, and P. O. Rasmussen, "Start-up problem with an induction machine and a permanent magnet gear," in *Proc. IEEE Energy Convers. Congr. Expo*, 2014, pp. 1348-1355.
[26] R. G. Montague, C. M. Bingham, and K. Atallah, "Magnetic gear dynamics for servo control," in *Proc. IEEE Mediterranean Electrotechnical Conf.*, 2010, pp. 1192-1197.